Optics Letters

OFC-enabled high-accuracy and real-time AMCW LiDAR for absolute laser ranging

Lihan Wang,[1,†] Qianwen Sang,[1,†] Xiaohu Tang,[1] Xudong Wen,[2] Haoran Wu,[1] Wei Zhang,[1] Yaoyao Shi,[1,3] Shupeng Li,[4] Yamei Zhang,[1] Xiangchuan Wang,[1,*] and Shilong Pan[1]

[1]National Key Laboratory of Microwave Photonics, Nanjing University of Aeronautics and Astronautics, Nanjing 210016, China
[2]Jiuquan Satellite Launch Center, Jiuquan 732750, China
[3]College of Physics, Nanjing University of Aeronautics and Astronautics, Nanjing 210016, China
[4]Suzhou LiuYaoSi Information Technologies Co., Ltd., Nanjing 211100, China
[†]These authors contributed equally to this Letter.
*wangxch@nuaa.edu.cn

Received 2 June 2025; revised 9 July 2025; accepted 9 July 2025; posted 10 July 2025; published 10 August 2025

An amplitude-modulated continuous-wave (AMCW) LiDAR based on an optical frequency comb (OFC) is proposed and demonstrated. We employ an OFC for ranging signal down-conversion, ensuring high ranging, accuracy, and speed while alleviating the requirements for large-bandwidth photodetectors (PDs) and high-performance analog-to-digital converters (ADCs). In addition, we intensity-modulate a reference electrical pulse sequence onto the OFC to extend the measurable range and eliminate range ambiguity according to the pulse time difference in the time domain. The experiments achieved a repeatability of 10.5 nm at an average time of 427 ms, an accuracy of ±0.8 μm, and an update rate of 150 Hz. Additionally, three-dimensional (3D) laser imaging, with a standard deviation (STD) of 3.7 μm, was achieved using a micro-electro-mechanical system (MEMS) scanning mirror.

https://doi.org/10.1364/OL.569508

Light detection and ranging (LiDAR) has emerged as an essential technology in modern industrial and scientific metrological applications due to its high precision, extended measurement range, and rapid acquisition capabilities. It has been widely used in three-dimensional mapping [1] and autonomous driving [2]. Current mainstream laser ranging techniques include direct time-of-flight (DToF) [3], frequency-modulated continuous wave (FMCW) [4], and amplitude-modulated continuous wave (AMCW) [5]. DToF enables long-distance detection, but its accuracy is constrained by the time-domain resolution of the system. The FMCW LiDAR offers high resolution and accuracy but suffers from complex and costly system architecture. In contrast, AMCW LiDAR eliminates the high requirement for frequency-tunable lasers and is less dependent on complex optical frequency modulation components, which reduces system complexity and hardware cost.

However, traditional AMCW LiDAR still faces the trade-off between accuracy, speed, and unambiguous range. To address this, Xu *et al.* [6] proposed a dynamic optical frequency comb (OFC) ranging method, achieving an accuracy of 25 μm at a distance of 65 m and a large non-ambiguous range through repetitive frequency scanning. Nonetheless, the measurement speed is limited by the heavy signal processing load. According to the fundamental theory in parameter estimation [7], when a fixed SNR is given, the only way to improve the Cramér–Rao Bound (CRB) is to increase the root-mean-square (RMS) bandwidth of the amplitude envelope. Extending the RMS bandwidth usually leads to an increased requirement in signal processing. To avoid directly processing high-frequency signal, photonic-based down-conversion [8,9] can be employed during the photoelectric conversion process. In this approach, the local oscillator (LO) and return radio-frequency (RF) signals are modulated onto an optical carrier via electro-optic modulation. Optical mixing then occurs in the photodetector (PD), directly generating the intermediate frequency (IF) signal while preserving the phase integrity. This method allows the use of a low-speed PD with high conversion gain. It also reduces the data throughput burden on the receiver and thereby enhances the measurement speed. For example, in Ref. [10], a 15-GHz amplitude envelope is down-converted to a 90-kHz electrical signal, enabling an AMCW LiDAR system to achieve sub-100-nm precision. However, this method requires sweeping the frequency of the amplitude envelope to extend the measurable range, which prevents real-time and large-range distance measurement. Researchers have utilized multi-tone signals [11], chirped signal [12], and pseudo-random codes [13] in AMCW LiDAR to eliminate the periodic ambiguity. However, these approaches typically demand higher computational resources, which challenges the AMCW systems to achieve high accuracy, fast speed, and absolute distance measurement simultaneously.

In this Letter, we propose a high-accuracy, real-time, and long-range AMCW LiDAR system that employs an optical frequency comb (OFC) as the measurement signal. The OFC inherently carries abundant frequency components, which

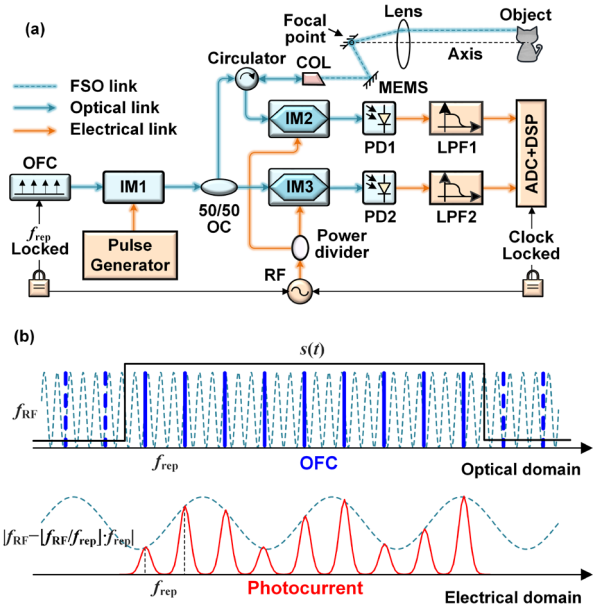

Fig. 1. (a) Schematic diagram of the proposed LiDAR system. (b) Time-domain features of the measurement signals. ADC, analog-digital converter; COL, collimator; DSP, digital signal processor; FSO, free-space optics; IM, intensity modulator; LPF, low-pass filter; MEMS, micro-electro-mechanical system; OC, optical coupler; OFC, optical frequency comb; PD, photodetector; RF, radio-frequency.

significantly increases the RMS bandwidth of the amplitude envelope. A photonic-based down-conversion is utilized to reduce the receiver's burdens. This simultaneously achieves high-speed and high-accuracy ranging. In addition, we intensity-modulate a reference electrical pulse sequence onto the OFC and extract the phase of the two frequencies through digital phase detection to extend the measurable range and eliminate range ambiguity. The proposed method effectively resolves the traditional AMCW LiDAR's trade-off among accuracy, speed, and unambiguous range.

The schematic diagram of the OFC-enabled AMCW LiDAR system is illustrated in Fig. 1(a). In the system, an OFC with a repetition frequency f_{rep} is first intensity-modulated by an intensity modulator (IM1) using a predefined electrical square wave pulse sequence. This modulation signal is characterized by a pulse width T_{w} and a repetition period T_{r}. The modulated OFC signal is then split into a reference optical branch and a probe optical branch via a 50:50 optical coupler (OC). The probe optical signal is transmitted through a free-space optics (FSO) link after collimation to enable LiDAR functionality. The reflected optical signal from the target is re-collimated into the fiber and directed to IM2. Simultaneously, the reference optical signal is injected into IM3. Both intensity modulators (IM2 and IM3) are driven by radio-frequency (RF) signals at a frequency f_{RF}.

The time-domain features and the electrical pulse sequence $s(t)$ are detailed in Fig. 1(b). Crucially, the OFC signal undergoes photonic undersampling in the optical domain at a rate of f_{rep}. This process maps the modulated RF signal onto the low-frequency envelope of the OFC, resulting in a down-conversion component with a frequency of $|f_{\mathrm{RF}} - f_{\mathrm{RF}}/f_{\mathrm{rep}} \cdot f_{\mathrm{rep}}|$, where $\ldots$ denotes the floor function.

Subsequently, the probe and reference optical signals are injected into PDs and filtered by electrical low-pass filters (LPF) separately. Based on the above analysis, the photocurrent contains the direct current (DC) component of the OFC and undersampled low-frequency envelope. For simplicity, we define a positive integer $N_1 = f_{\mathrm{RF}}/f_{\mathrm{rep}} + 1$. Since the phase values are directly extracted with the range of $-\pi$ to π, the phase shift of these frequency components between the probe signal and the reference signal can be expressed as:

$$\varphi_{\mathrm{rep}} = -2\pi f_{\mathrm{rep}}\tau + 2\pi\left\lfloor \frac{1}{2} + f_{\mathrm{rep}}\tau \right\rfloor, \tag{1}$$

$$\varphi_{\mathrm{env}} = -2\pi N_1 f_{\mathrm{rep}}\tau + 2\pi\left\lfloor \frac{1}{2} + N_1 f_{\mathrm{rep}}\tau \right\rfloor, \tag{2}$$

where τ is the transfer delay of the FSO link. The floor functions in Eqs. (1) and (2) represent the phase-wrapping terms. To obtain the absolute laser ranging result, we propose a novel two-step phase-unwrapping algorithm. First, Eq. (1) can be reorganized as:

$$\left\lfloor \frac{1}{2} + f_{\mathrm{rep}}\tau \right\rfloor = \frac{\varphi_{\mathrm{rep}}}{2\pi} + f_{\mathrm{rep}}\tau. \tag{3}$$

In Eq. (3), the right-hand term of the equation should always equate to an integer. Therefore, we can make an approximate estimation that [14]:

$$\left\lfloor \frac{1}{2} + f_{\mathrm{rep}}\tau \right\rfloor = \left\lfloor \frac{\varphi_{\mathrm{rep}}}{2\pi} + f_{\mathrm{rep}}\tau_{\mathrm{rou}} + \frac{1}{2} \right\rfloor, \tag{4}$$

where τ_{rou} is the rough time delay, which is estimated from the time-domain pulse difference between the reference and measurement path. Assuming the errors in τ_{rou} and φ_{rep} are $\Delta\tau$ and $\Delta\varphi$, respectively, Eq. (4) holds if and only if the following condition is satisfied [14]:

$$\left| f_{\mathrm{rep}}\Delta\tau + \frac{\Delta\varphi}{2\pi} \right| < \frac{1}{2}. \tag{5}$$

By combining Eqs. (1) and (4), we obtain:

$$\tau' = \frac{1}{f_{\mathrm{rep}}}\left\lfloor \frac{1}{2} + f_{\mathrm{rep}}\tau_{\mathrm{rou}} + \frac{\varphi_{\mathrm{rep}}}{2\pi} \right\rfloor - \frac{\varphi_{\mathrm{rep}}}{2\pi f_{\mathrm{rep}}}, \tag{6}$$

where τ' denotes the FSO transfer delay derived based on repetition frequency f_{rep}. Similarly, we can repeat the process to determine the FSO transfer delay:

$$\tau_{\mathrm{mea}} = \frac{1}{N_1 f_{\mathrm{rep}}}\left\lfloor \frac{1}{2} + N_1 f_{\mathrm{rep}}\tau' + \frac{\varphi_{\mathrm{env}}}{2\pi} \right\rfloor - \frac{\varphi_{\mathrm{env}}}{2\pi N_1 f_{\mathrm{rep}}}. \tag{7}$$

Equation (7) holds if and only if the following condition is satisfied:

$$\left| N_1 f_{\mathrm{rep}}|\tau - \tau'| + \frac{\Delta\varphi}{2\pi} \right| < \frac{1}{2}. \tag{8}$$

If Eq. (5) is satisfied, then we can make an approximation that $|\tau' - \tau| \approx \Delta\varphi/2\pi f_{\mathrm{rep}}$. Therefore, Eq. (8) can be further written as:

$$|\Delta\varphi| < \frac{\pi}{N_1 + 1}. \tag{9}$$

Finally, the unambiguous distance of the FSO link can be calculated using the formula: $d = c \times \tau_{\mathrm{mea}}/2n_{\mathrm{air}}$. Here, the group

refractive index of air (n_{air}) was 1.000262, estimated by the Ciddor equation (T:25°C, P: 1008 hPa, RH: 45%) [15], and c is the speed of light in the vacuum. Based on the above analysis, if Eqs. (5) and (8) are satisfied, the ranging accuracy of LiDAR can be expressed as:

$$\Delta d = c\frac{\Delta\varphi}{4n_{\mathrm{air}}\pi N_1 f_{\mathrm{rep}}}. \tag{10}$$

From Eq. (8), it can be derived that increasing the frequency of the RF signal will correspondingly increase the value of N_1. This, in turn, improves the ranging accuracy of the LiDAR system. Moreover, this operation does not impose additional bandwidth or data volume burdens on the receiver, owing to the photonic-based down-conversion. The repetition frequency f_{rep} directly affects the frequency range after down-conversion, and the selection of f_{rep} and f_{RF} must consider practical engineering constraints.

A proof-of-concept experiment is conducted based on the setup illustrated in Fig. 1(a). The mode-locked laser (Menlo Systems, C-Fiber) generates an OFC signal with a pulse width of less than 90 fs, an average power of approximately 20 dBm, and a repetition rate of 100.3997 MHz. The OFC signal is first modulated by an acoustic-optic modulator (Gooch & Housego). The driving electrical pulse signal, with a pulse width of 3.95 μs, a repetition cycle of 4 μs, and a center frequency of 200 MHz, is generated by an arbitrary waveform generator (Keysight M9505A). Therefore, the unambiguous range of the LiDAR system exceeds 599.42 meters, which can be calculated by c×4 μs/2/n_{air}. Two 40-GHz IMs (Fujitsu, FTM7938) are employed to modulate the OFC signals, driven by an RF signal at 39.9845 GHz generated from a microwave source (RS, SMA100B). Two 20-GHz PDs (Picometrix, P-18A) convert the optical signals into photocurrents. The PD offers a bandwidth on the order of several hundred MHz, which is sufficient. The signals are subsequently filtered using two LPFs (Talent Microwave, Inc., TLLF-DC-500M-L), with a cutoff frequency of 500 MHz. The rough delay is determined from the time-domain waveform of the photocurrents, which is sampled by a 10-bit data acquisition card operating at a sampling rate of 1.25 GSa/s.

The stability of the proposed LiDAR system is first evaluated. A fundamental trade-off exists between the refresh rate and ranging accuracy. To maintain the sub-micron-level accuracy, the refresh rate is constrained to 150 Hz. Figure 2(a) illustrates the system's fluctuation measured at a refresh rate of 150 Hz over 66 seconds, without the LiDAR system connected to the FSO link and IM1 is off. The measured distance fluctuation remains within ±0.5 μm with a standard deviation (STD) of 0.1592 μm. The Allan deviations of the system are presented in Fig. 2(b), reaching 10.5 nm at an average time of 427 ms. This result is comparable to the most OFC-based LiDAR ranging systems.

To evaluate the ranging accuracy, a manual translation stage equipped with a reflected mirror is employed to perform measurements at 5 μm intervals. As illustrated in Fig. 3(a), the measured distances exhibit a strong linear correlation with the preset equidistant intervals. Figure 3(b) further demonstrates that the measurement accuracy remains within ±0.8 μm.

To validate the absolute laser ranging capability of the proposed LiDAR system, a 26-meter single-mode fiber is selected as the optical link under test. Figure 4(a) shows the frequency spectrum of the photocurrent signal measured using a spectrum analyzer (Rohde Schwarz, FSV). It can be calculated that N_1 = 39.9845 GHz/100.3997 MHz +1 = 399.

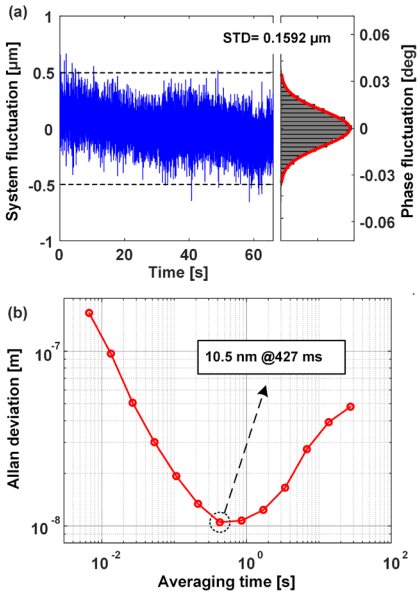

Fig. 2. (a) System's fluctuation and histogram over 66 seconds. (b) Measurement repeatability in terms of the Allan deviation.

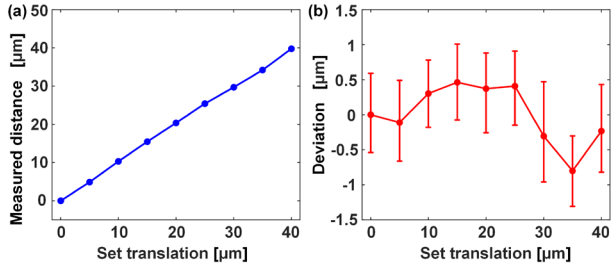

Fig. 3. Measured distance of the manual translation stage. (a) Measured distance of the displacement stage with 5 μm steps. (b) Distance deviation.

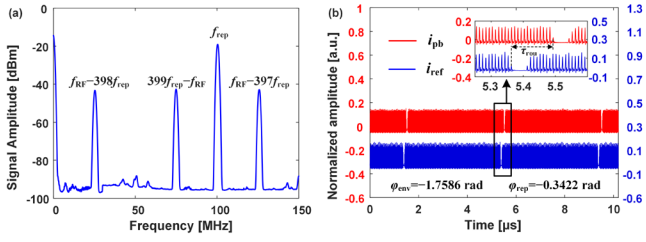

Fig. 4. (a) Frequency spectrum of the reference photocurrent signal. (b) Time-domain waveform of the probe photocurrent and reference photocurrent.

Therefore, the frequency components in Fig. 4(a) are $f_{\mathrm{RF}} - 398f_{\mathrm{rep}}$, $399f_{\mathrm{rep}} - f_{\mathrm{RF}}$, f_{rep}, and $f_{\mathrm{RF}} - 397f_{\mathrm{rep}}$, respectively. To implement the two-step phase-unwrapping algorithm, according to Eq. (5), the rough delay error must satisfy $|\Delta\tau| < 1/(2f_{\mathrm{rep}}) = 4.98$ ns. Given the sampling rate of 1.25 GSa/s, the rough delay error in a high SNR scenario would be below 0.8 ns, satisfying the first constraint condition. To meet the second constraint condition, the phase error $\Delta\varphi$ should be less than $180°/(N_1+1) = 0.45°$. As shown in Fig. 2(a), the phase error is better than 0.05°, which satisfies the phase-unwrapping algorithm condition.

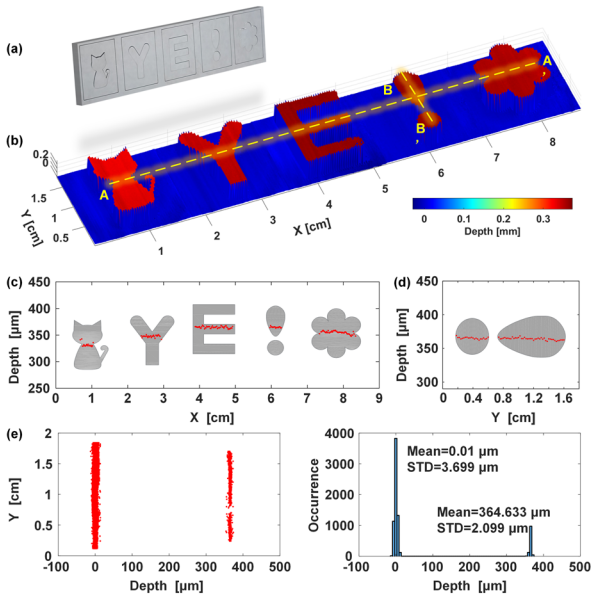

Fig. 5. (a) Picture of the to-be-tested sample. (b) Measured morphologic map of the sample. (c) Depth extraction results along the A–A′ direction. (d) Depth extraction results along the B–B′ direction. (e) Measured "!" pattern profile curves in the x direction and its histogram.

Figure 4(b) illustrates the time-domain waveforms of photocurrents. From the modulated electrical pulse sequence, the rough time delay can be calculated as τ_{rou} = 13/100.3997 MHz = 129482.588 ps (corresponding to a 25.896518-meter fiber). The phase shifts of φ_{env} and φ_{rep}, corresponding to the frequencies of $399f_{\mathrm{rep}} - f_{\mathrm{RF}}$ and f_{rep}, are extracted as $\varphi_{\mathrm{env}} = -1.7586$ rad and $\varphi_{\mathrm{rep}} = -0.3422$ rad, respectively. Consequently, we obtain $\tau' = 130024.919$ ps. The precise unambiguous transfer delay of the optical link is calculated as 130013.666 ps (corresponding to a 26.002733-meter fiber), validating the system's capability for absolute distance measurement.

Finally, we perform a 3D imaging based on the proposed LiDAR system. A custom stainless-steel workpiece with a 12k fine-polished surface is prepared, as shown in Fig. 5(a). The workpiece has a thickness of approximately 0.33 cm, and each pattern measures about 12 mm × 15 mm. The actual optical coupling efficiencies during the measurements ranged from 7.9% to 21.5%. The reduction in optical power leads to a certain decrease in the measurement accuracy. In the LiDAR system, the laser beam is controlled by MEMS (Mirrorcle, MEMS Mirrors). The output of the MEMS beam is positioned at the focal point of a convex lens; therefore, the rotation of the MEMS directs the beam to specific positions on the pattern. In our system, the MEMS mirror implements a 100 × 100 raster scanning pattern to spatially sample the pattern area with a lateral resolution of 0.12 mm. During the scanning process, the depth information corresponding to each scanning point is simultaneously calculated to reconstruct 3D profiles of the targets. The refined 3D imaging results are depicted in Fig. 5(b), demonstrating that the letters can be clearly resolved. In detail, the measured depths along the A–A′ direction and the B–B′ direction are plotted in Figs. 5(c) and 5(d), respectively. The measured depths accurately reflect the real height of the patterns. Figure 5(c) shows the depth extraction results along the A–A′ direction in Fig. 5(b). Figure 5(d) presents the depth extraction results along the B–B′ direction in Fig. 5(b), and Fig. 5(e) displays the measurement histogram and its standard uncertainty for the "!" pattern. The above results show that the proposed method can realize high-accuracy 3D imaging with an STD of the measured depth better than 3.7 μm.

In summary, a high-performance AMCW LiDAR system based on OFC is proposed and demonstrated. The photonic-based down-conversion technique effectively alleviates the receiver's burdens, enabling high-accuracy, ambiguity-free, and real-time laser ranging. The demonstrated system exhibits significant potential for applications in autonomous navigation and industrial metrology applications, where micron-scale accuracy, absolute distance measurement, and hundred-Hz class refresh rates are required.

Funding. National Natural Science Foundation of China (62271249); Fundamental Research Funds for the Central Universities (NC2024004).

Disclosures. The authors declare no conflicts of interest.

Data availability. Data underlying the results presented in this paper can be obtained from the authors upon reasonable request.

REFERENCES

1. J. Liu, D. Xu, J. Hyyppä, *et al.*, IEEE J. Sel. Top. Appl. Earth Obs. Remote Sens. **14**, 5627 (2021).
2. Y. Li and J. Ibanez-Guzman, IEEE Signal Process. Mag. **37**, 50 (2020).
3. F. Taneski, T. A. Abbas, and R. K. Henderson, J. Light. Technol. **40**, 5884 (2022).
4. R. Wang, C. F. Cheung, C. Wang, *et al.*, IEEE Trans. Instrum. Meas. **72**, 2520010 (2023).
5. C. Zhang, Z. Zhang, Y. Tian, *et al.*, IEEE Trans. Instrum. Meas. **70**, 8500711 (2021).
6. X. Xu, Z. Zhang, H. Zhang, *et al.*, Opt. Express **28**, 4398 (2020).
7. R. N. McDonough and A. D. Whalen, *Detection of Signals in Noise* (Academic Press, 1995).
8. Z. Tang, Y. Li, J. Yao, *et al.*, Laser Photonics Rev. **14**, 1800350 (2020).
9. B. Li, W. Wei, D. Han, *et al.*, Opt. Express **28**, 12588 (2020).
10. Y.-S. Jang, J. Park, and J. Jin, Opt. Express **29**, 12229 (2021).
11. L. Wang, X. Wang, X. Liu, *et al.*, Photon. Res. **13**, 1302 (2025).
12. Z. Zhang, T. Shirahata, R. Chen, *et al.*, Opt. Express **31**, 26577 (2023).
13. A. Rybaltowski and A. Taflove, Opt. Lett. **29**, 1709 (2004).
14. L. Wang, Y. Yang, Q. Sang, *et al.*, J. Light. Technol. **43**, 4538 (2025).
15. P. E. Ciddor, Appl. Opt. **35**, 1566 (1996).